Numerical modeling of resistive switching in RRAM device.

D. Niraula*, V. Karpov
Department of Physics and Astronomy, The University of Toledo, Toledo, OH, USA
*Corresponding author: 2801 W. Bancroft St., MS 111, Toledo, OH, 43606, USA
dipesh.niraula@rockets.utoledo.edu

Abstract: Numerical modeling based on thermodynamics of phase transitions is used to emulate resistive switching (RS) phenomena in resistive random access memory device and to reproduce unique features of the current-voltage (I-V) characteristics corresponding to RS. The numerical technique calculates the free energy (FE) of the device, and finds a stable phase configuration of the device during RS. COMSOL Multiphysics® simulation software package is utilized to compute the electric field and temperature distributions that are necessary to find the device FE, and MATLAB® package, via LiveLink™ to MATLAB®, is utilized to find the stable phase configurations for various source voltages. The corresponding electric current and voltage are then computed. The generated approximate I-V correctly represent the observed non-trivial trends.

Keywords: Device Modeling, RRAM, Resistive Switching, Thermodynamics of Phase Transitions.

1. Introduction

RS refers to the sudden transformation of insulator into conductor and vice-versa, under a strong electric field or current. RS is a non-volatile and reversible process, which can be applied to create a memory device. One of the application of RS is the newly emerging nanoscale resistive random access memory (RRAM), which is a metal-insulator-metal multilayered capacitor like device. RS in RRAM is caused by the formation and dissolution of a cylindrical conducting filament (CF) in its insulating layer. Formation of CF corresponds to conducting low resistance state (LRS) whereas dissolution of CF corresponds to insulating high resistance state (HRS). LRS and HRS of RRAM are equivalent to the logical ‘0’ and ‘1’ binary states. The non-volatile binary states make RRAM a promising memory device.

A typical I-V characteristics of RRAM device is presented in Figure 1 which shows two peculiar domains corresponding to RS: (i) the fast voltage snapback domain A-B followed by the vertical domain B-C, and (ii) the fast voltage snapforward domain D-E followed by the horizontal domain E-F. The former corresponds to RS from HRS (OFF state) to LRS (ON state) called SET process, whereas the latter corresponds to RS from LRS to HRS called RESET process. In addition, domains C-0-D and A-0-F in Figure 1 corresponds to LRS and HRS respectively.

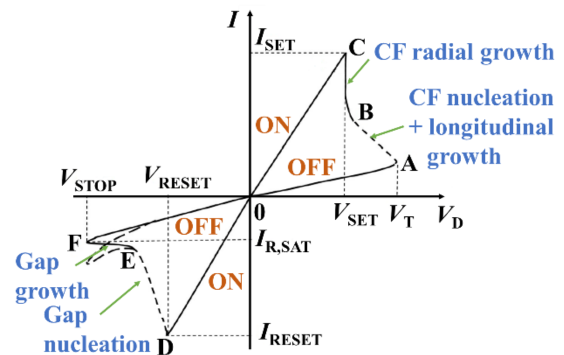

Figure 1. Representation of a typical I-V characteristics of RRAM [1]-[4]. V_D is the voltage across the device different from the source voltage V_S due to an external load resistor in series. The SET current I_{SET} is defined by the maximum current limit called compliance current. The dashed domain represents very fast nucleation process. Note: the peculiar voltage snapback and snapforward is not present in I-V characteristic corresponding to source voltage.

Numerous microscopic models [5]-[8] have been proposed to explain RS. The switching mechanism of those models are based on field and/or temperature induced migration of ions and defects in the insulator layer of RRAM. In contrast, a recently proposed phenomenological theory, [9], [10] based on the thermodynamics of phase transitions, defines RS through macroscopic processes of phase transitions. That thermodynamic theory utilizes material parameters to describe different phases into which the insulating layer transforms, during phase transitions underlying RS. The transitions between three phases: (i) stable insulating (i-phase), (ii) metastable conductive (mc-phase), and (iii) unstable conductive (uc-phase) are involved. CF is composed of metastable conducting phase which transforms to stable insulating phase during dissolution of CF via unstable conductive phase and vice-versa during formation of CF. For numerical modeling, information about the difference in chemical potentials between different

phases is sufficient to apply the thermodynamic description. A quantitative analysis of the thermodynamic model is presented in Ref. [10].

The goal of this paper is to present the numerical technique, based on the thermodynamic theory, employed to obtain the I-V characteristics of RRAM device during RS process.

2. Thermodynamic Model

The thermodynamic model is based on the principle of minimum free energy, which can be paraphrased as: free energy (FE) of RRAM device increases due to applied power source; in response, the device evolves in such a way as to minimize its FE through the process of phase transition.

RRAM is composed of a thin insulating metal oxide layer sandwiched in between two metal electrodes, as illustrated in Figure 2. A mere voltage bias of 1 V across the thin insulator layer of 5 nm creates a strong electric field of 200 MV/m. Due to that electric field the insulator layer gains substantial amount of electrostatic energy. In response, the insulating layer locally transforms into conducting phase forming a cylindrical CF as shown in Figure 2(i). It releases the stored electrostatic energy by conducting electricity. This phase transformation is triggered by field induced nucleation (FIN) [11] at the threshold field, corresponding to the threshold voltage V_T (Point A in Figure 1). The electroformed nucleus then grows longitudinally into a needle shaped filament, shunting the device. Nucleation and longitudinal growth of the CF is a fast process, during which the device voltage drops (snapback), and the current flow increases (domain A-B in Figure 1) due to the sudden decrease in device resistance. The electrostatic energy falls considerably after shunting, which locally suppresses growth to any other CF.

Although CF conducts electricity, it also charges due to its nonzero capacitance and resistance. The charged CF produces a strong radial electric field in its vicinity. This radial electric field then polarizes its surrounding as shown in Figure 2(ii). Simultaneously, the system gains thermal energy via Joule Heating due to the flow of current through CF. As a result, CF grows radially to a stable radius corresponding to the minimum device FE. Further increase in power transforms CF toward larger radius.

After shunting, raising power source barely raises the device voltage because the load resistance dominates the device resistance (R_L>>R_D). The current increases with radially growing filament (decreasing filament resistance). This corresponds to the vertical I-V domain B-C in Figure 1 where the current grows for a fixed device voltage, V_{SET}. In addition, the full-grown CF's radius is set by the highest current through the device (I_{SET} in Figure 1).

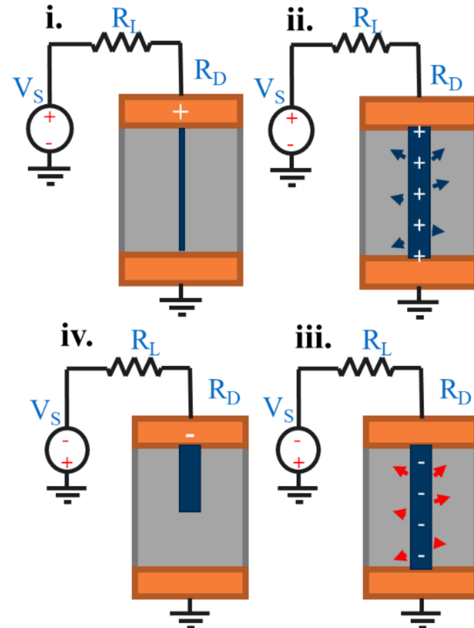

Figure 2. Formation and dissolution of CF in a generic metal-insulator-metal multilayered RRAM device. V_S is the source voltage, R_L is the load resistance, and R_D is the device resistance. The arrows represent polarization of the insulating host near CF; blue (ii) and red (iii) color denotes energetically favorable and unfavorable states, respectively. Note: the pictures are placed in a cyclic order corresponding the SET and RESET RS cycle.

In bipolar RS, the power source polarity is reversed to switch the device back to its OFF/HRS state. During SET process, the charged CF polarizes its surrounding. This polarization retains when the power source is disconnected. Reversing the polarity of the power source charges CF opposite to that in the SET process. CF now opposes the inherited surrounding polarization as shown in Figure 2(iii) and the system gains electrostatic energy. The insulating polarization and the metastable CF unfreezes when the device voltage equals to V_{SET} in magnitude, which is called reset voltage ($V_{RESET,}$ point D in Figure 1). This triggers phase transformation of conducting phase back to insulating phase, dissolving the CF as shown in Figure 2(iv). The thermodynamic model describes this process as nucleation of a gap, where the voltage snaps forward and current drops instantaneously due to abrupt increase in the device resistance (domain D-E in Figure 1). After RS to OFF state, the device resistance dominates the load resistance (R_D>>R_L).

Increasing the voltage source increases the gap length and the currents saturates represented by $I_{R,SAT}$.

3. Numerical Model

RS corresponding to SET process is composed of two sub processes: fast shunting of electrodes followed by the radial growth of CF. Shunting can be further divided into nucleation and longitudinal growth of CF, which are stochastic in nature. Similarly, RS corresponding to RESET process is also composed of two sub processes: nucleation of gap and growth of the gap where the nucleation of gap is of stochastic nature. It is not immediately clear how to model such stochastic processes with COMSOL hence, solving that problem is beyond the scope of this paper. Here, numerical modeling is presented for radial growth of CF, which corresponds to I-V domain B-C in Figure 1, and growth of gap, which corresponds to I-V domain E-F in Figure 1.

The device under consideration is TiN/Hf/HfO2/TiN multi-layered RRAM having a cross-sectional area of 20nm×20nm as reported in [1] and [12]. However, a cylindrical device of 10 nm radius as shown in Figure 3 was considered instead to reduce the 3D to 2D geometry by exploiting the rotational symmetry about the longitudinal axis of the cylindrical shape.

We consider FE of the device in (Eq. (31), Ref. 6)

$$F = \int \rho C_P \delta T dx^3 + \frac{1}{2}\int \epsilon |E|^2 dx^3 + 2\pi r h \sigma_s + \pi r^2 h \delta\mu \quad (1)$$

where, ρ is the mass density, Cp is the specific heat capacity at constant pressure, δT is the change in temperature, ε is the permittivity, $\boldsymbol{E}$ is the electric field, r is the radius, h is the CF height (l for gap length), σ_s is the interfacial energy, and $\delta\mu$ is the difference in chemical potential between uc-phase and i-phase during SET process ($\delta\mu_1$) and between uc-phase and mc-phase during RESET process ($\delta\mu_2$). The first and second terms in Eq. (1) represent thermal and electrostatic energy, while the last two terms correspond to the phase transformation energy which applies only to filament/gap. Furthermore, the electrostatic energy (also expressed as $CV^2/2$, where C is the capacitance) of the conductive component (electrodes and filament), is negligible compared to the insulator layer due to higher capacitance, hence the insulator layer dominates the electrostatic contribution to the total FE. Conversely, conductors dominate the thermal contribution due to larger current flow.

The minimum FE configuration of the device and its corresponding I-V characteristics is found utilizing numerical technique based on following algorithm.

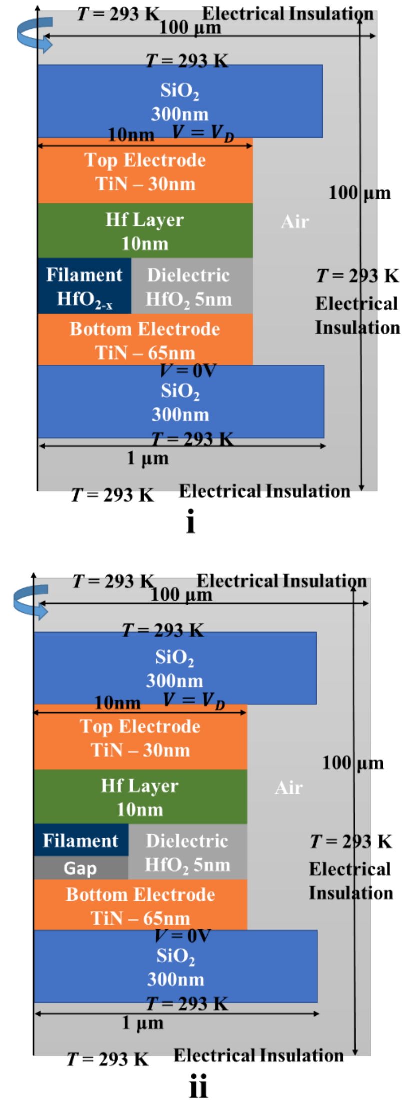

Figure 3. Schematic of multilayer RRAM cross-section. Figures 3(i) and 3(ii) correspond to model used to emulate SET and RESET process respectively. The figures include geometric parameters and material names of the device's various layers, and the boundary conditions. The gap in the second figure was modeled as HfO_2. Note: Figure not drawn to scale.

i. construct a device
ii. fix the source voltage and calculate device FE for all range of filament radii, 0 to device radius, and for all range of gap lengths, 0 to insulator thickness
iii. find the minimum in FE w.r.t CF radius (∂F/∂r) and gap length (∂F/∂l) for a fix source voltage
iv. redo step 2 and 3 for all range of source voltages
v. record the device voltage and CF radius/gap length corresponding to the FE minimum for all source voltages

vi. calculate the current for device voltages and CF radius/gap length recorded in step 5

vii. two sets of I-V are obtained in step 6 that represent vertical B-C domain and horizontal E-F domain of the I-V plot of Figure 1

3.1 COMSOL Multiphysics

Two devices were constructed in *2D axisymmetric* mode in COMSOL for SET and RESET process as shown in Figures 3(i) and 3(ii) respectively. The use of 2D geometry reduces the volume integrals in Eq. (1) to area integrals in following Eq. (2.1) and Eq. (2.2) corresponding to SET and RESET process respectively.

$$F_{SET} = \iint \rho C_P \delta T drdz + \frac{1}{2}\iint \epsilon |E|^2 drdz + 2\pi rh\sigma_s + \pi r^2 h\delta\mu_1 \quad (2.1)$$

$$F_{RESET} = \iint \rho C_P \delta T drdz + \frac{1}{2}\iint \epsilon |E|^2 drdz + 2\pi rl\sigma_s + \pi r^2 l\delta\mu_2 \quad (2.2)$$

To calculate the device FE in Eq. (2), the electric field distribution ($\boldsymbol{E}$) and temperature distribution (T) must be known. Numerous partial differential equations were solved in COMSOL to obtain $\boldsymbol{E}$ and T which are listed below in its respective COMSOL module utilized in the numerical model.

i. *Electric Currents* module

$$\boldsymbol{\nabla}.\boldsymbol{J} = 0, \quad \boldsymbol{J} = \sigma\boldsymbol{E}, \quad \boldsymbol{E} = -\nabla V \quad (3)$$

ii. *Heat Transfer in Solids* module

$$-\kappa\nabla^2 T = Q_s \quad (4)$$

iii. *Multiphysics* module

$$Q_s = \boldsymbol{J}.\boldsymbol{E} \quad (5)$$

where $\boldsymbol{J}$ is the current density, σ is the electric conductivity, κ is the thermal conductivity and Q_s is the heat source. Equations in Eq. (3) are the current conservation law, Ohms law, and the relation between electric field and electric potential due to Maxwell law respectively. Equation (4) is the Fourier heat law where the heat source is provided by the Joule heat term in Eq. (5). Furthermore, the *Multiphysics* module couples the *Electric Currents* and *Heat Transfer in Solids* modules to define the electromagnetic heat source.

Table 1: Material Parameters [13]-[18]

Material	TiN	HfO_2	HfO_{2-x}	Hf	SiO_2	Air
Thermal Conductivity (κ) [W/K.m]	11.9	0.5	0.65 [a]	23	1.38	0.015
Electrical Conductivity (σ) [S/m]	10^6	10 [e]	2×10^4 [b]	5×10^6	10^{-14}	5×10^{-15}
Specific Heat Capacity (C_P) [J/kg.K]	545	120	140 [c]	144	703	1000
Relative Permittivity (ε_r)	$-\infty$ [d]	25	$-\infty$ [c,d]	$-\infty$ [d]	3.9	1
Density (ρ) [kg/m^3]	5.22×10^3	10×10^3	12×10^3 [c]	13.3×10^3	2.2×10^3	1.225

[a] Estimated as a sum of the electron and lattice components, where electronic component is calculated via Wiedemann-Franz-Lorenz law

[b] Calculated from the device I-V [2] assuming the truncated cone shaped CF of radii $r_> \sim 5$ nm and $r_< \sim 3$ nm [19]

[c] Assumed value such that it lies in between Hf and HfO_2

[d] -10^6 was used instead of $-\infty$ for practical purpose

[e] Assumed to change after the forming process

Table 2: Various Parameters [10], [13], [20]

Parameters	Value
Interfacial Energy (σ_s)	0.01 J/m^2
Chemical Potential ($\delta\mu_1, \delta\mu_2$) [f]	5×10^9 J/m^3
Load Resistor (R_L)	15 kΩ
TBR HfO_2 ($R_{b\ HfO2}$)	3 m^{2}K/GW
TBR TiN ($R_{b\ TiN}$)	5 m^{2}K/GW

[f] In reality, $\delta\mu_1, \delta\mu_2$ can have different values

The boundary conditions required to solve the differential equations are listed below.

i. *Electric Insulation* ($\boldsymbol{n}.\boldsymbol{J} = 0$)
All three boundaries of the air domain are electrically insulated. Here $\boldsymbol{n}$ is the unit vector normal to the surface boundary.

ii. *Ground (V = 0)*
Interface common to the bottom electrode and SiO_2 substrate is grounded.

iii. *Electric Potential* ($V = V_D$)
Interface common to the top electrode and SiO2 superstrate is provided with device voltage V_D.

iv. *Temperature* ($T = 293.15$ K)
Free surfaces of both SiO2 layers are placed at room temperature, assuming they are in contact with a larger body which acts as a heat sink and maintains room temperature. Also, all three boundaries of the air domain are at room temperature.

v. *Diffuse Surface* ($-\boldsymbol{n}.\boldsymbol{q} = \sigma_B (T_{amb}^4 - T^4)$)
All the interface and boundary of the device loses heat through radiation governed by Stefan-Boltzmann law. Here q is the power radiated per

surface area, σ_B is the Stefan-Boltzmann constant, and T_{amb} is the ambient temperature (293.15 K).

vi. *Thin Layer* ($-\mathbf{n}_d.\mathbf{q}_d=-(T_u-T_d)/R_b$)
Thermal boundary resistance (TBR) was assigned to all the interfaces of the device. TBR value of an interface depends on both layer that forms the interface; due to lack of data, the interfaces with HfO_2 and TiN on one side is assigned with a value from [14] and [20], respectively. For the common TiN/HfO_2 junction TBR value for HfO_2 was assigned. The u and d subscript in the *Thin Layer* equation represents either sides of an interface, and R_b is the TBR value.

In addition, the values of the coefficients of the differential equations and FE used for this modeling are listed in Table 1 and 2.

3.2 Circuitry

A load resistor is connected in series as shown in Figure 2, to prevent the device from excess current during RS. During SET process, the electroformed CF sets the resistance of the device. The device resistance and device voltage during SET process are given by following equations.

$$R_D = \frac{h}{\sigma_{\text{fil}}\pi r^2}, \qquad V_D = \frac{V_S}{1+\frac{R_L}{R_D}} \qquad (6)$$

During RESET process, the formation of gap changes the resistance of the device which is now given by the series combination of the partial filament and the gap. The electric field at the tip of the filament is enhanced due to the lightning rod effect so majority of current passes through the filament. Since the current takes the shortest route from the bottom electrode to the filament, the gap, through which the current passes, is considered as a cylindrical path of radius equal to that of the filament. Hence, the filament and gap resistance are given by,

$$R_{\text{fil}} = \frac{h-l}{\sigma_{\text{fil}}\pi r^2}, \qquad R_{\text{gap}} = \frac{l}{\sigma_{\text{gap}}\pi r^2} \qquad (7)$$

and the device resistance $R_D = R_{fil} + R_{gap}$. The device voltage during RESET process is also given by Eq. (6). Notice V_D is one of the boundary condition required to the solve the differential equations mentioned above.

3.3 MATLAB Scripts

MATLAB was used to find the minimum/stable FE configuration after calculating device FE in COMSOL using LiveLink to MATLAB which provides a platform to communicate with COMSOL solver. The device model can be constructed directly in COMSOL or through a MATLAB script which asks COMSOL to build the desired model. The latter was chosen for faster work flow between various MATLAB scripts presented as a flowchart in Figure 4. Scripts RRAM SET.m/RRAM RESET.m builds the device model, assigns material parameters to their respective domains, adds the required COMSOL physics module, sets all the required boundary conditions, and solves the differential equations to get electric field and temperature distribution for calculating the device FE. However, scripts I_V_SET.m/I_V_RESET.m controls the work flow. Script I_V_SET.m/I_V_RESET.m is run in MATLAB environment, which calls RRAM_SET.m/RRAM_RESET.m numerous times as needed, calculates FE and stable filament radius/gap length, and stores all the necessary information in DATA_SET.mat/DATA_RESET.mat MATLAB variable. Script Plot_SET.m/Plot_RESET.m extracts data from MATLAB variable DATA_SET.mat /DATA_RESET.mat and plots desired graph including I-V.

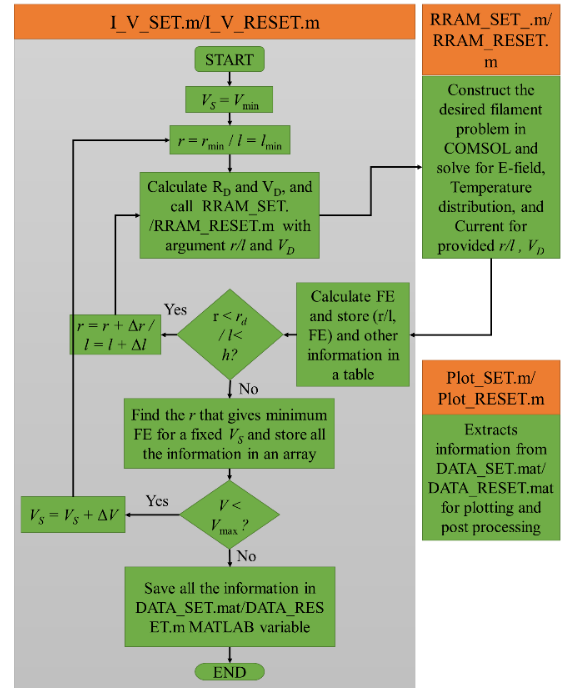

Figure 4. Flowchart defining the work flow between various MATLAB scripts. V_{min}, V_{max}, r_{min}/l_{min}, r_{max}/l_{max} and $\Delta r/\Delta l$ are user input variables. Note: r/l is not division but choice between CF radius r or gap length l.

4. Simulation Results and Discussion

The simulation results obtained from the MATLAB scripts Plot_SET.m and Plot_RESET.m are presented in Figure 5; Figures 5(i) and 5(ii) represents the vertical domain B-C and horizontal domain E-F of RRAM I-V characteristics, Figures 5(iii) and 5(v) compares device FE for four different source voltages,

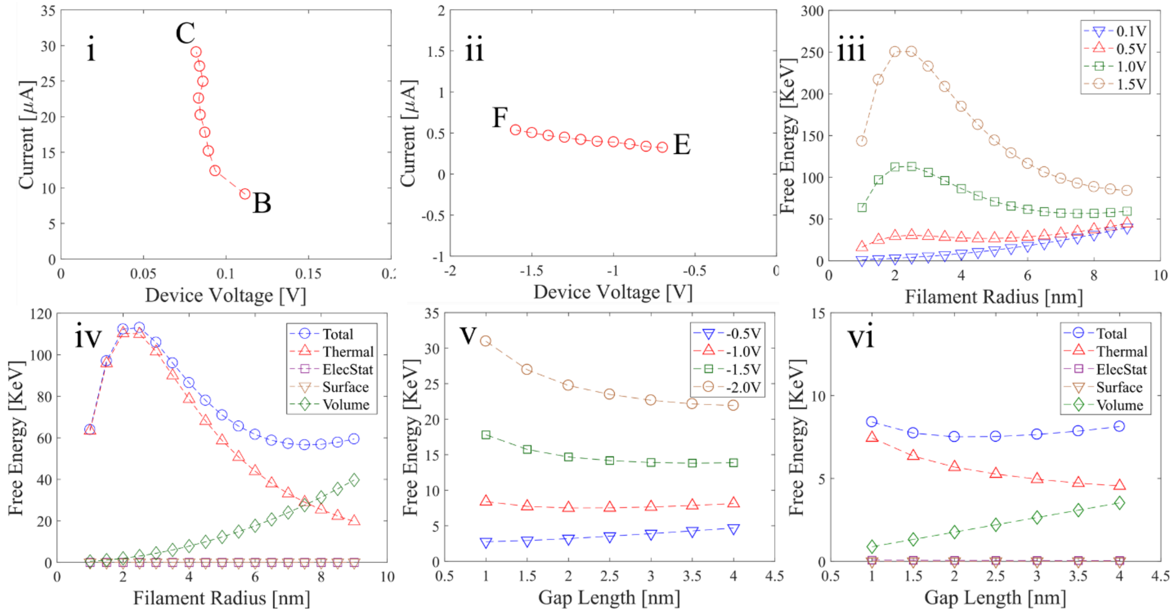

Figure 5. Simulated I-V and FE plots corresponding to the SET and RESET numerical solution are presented. Notice that the current axis of Figure 5(i) is presented in its absolute value. Figures 5(iv) and 5(vi) compare the FE contribution for source voltage of 1.0 V and -1.0 V respectively.

and Figures 5(iv) and 5(vi) compares the partial FE contribution to the total FE for SET and RESET processes respectively.

Each point of I-V characteristics in Figures 5(i) and 5(ii) corresponds to a stable CF radius and stable gap length respectively. The SET voltage V_{SET} in Figure 5(i) is found to be smaller than the experimental V_{SET} ~0.5V [1]. Two possible reasons for the underestimation of V_{SET} are: 1) unaccounted source of voltage drop within the device; most likely in the interface between dissimilar material (interface resistance, contact potential) and 2) overestimating the electrical conductance of the CF by assuming the filament to be one continuous metallic domain; it is known that the conductance of the CF shows a poor temperature dependence (not thermally activated) [21], which leaves room for the assumptions that CF might be composed of both dominating conducting phase, and insulating phase inclusions. Similarly, the saturating current, $I_{R,SAT}$ in Figure 5(ii) is smaller than the experimental $I_{R,SAT}$ ~25μA [1]. The gap was assumed to be composed of single insulating phase but it might contain both dominating insulating phase and conducting phase inclusions. In addition, tunneling current might be a significant conduction mechanism through the nanoscale gap and should be considered.

FE curves in Figures 5(iii) and 5(v) shows that smaller voltage cannot sustain the growth of the CF/gap while the stable CF radius/gap length for higher voltages lie outside the device dimension. For instance, FE curves corresponding to V_S of 0.1V in Figure 5(iii) and -0.5V in Figure 5(v) have no stable CF radius or gap length, whereas the stable radius and gap length for FE curves corresponding to V_S of 1.5V in Figure 5(iii) and -2.0V in Figure 5(v) lie beyond the device dimension. However, for the intermediate FE configurations the stable CF radius and gap length fall inside the device dimension; the stable CF radius corresponding to V_S of 0.5V and 1.0V in Figure 5(iii) are 4.8nm and 7.5nm, and the stable gap lengths corresponding to V_S of 1.0V and -1.5V in Figure 5(v) are 2.2nm and 3.6nm.

FE plot of Figure 5(iii) also shows that the stable CF radius increases with increasing V_S or current. This explains the observations that CF radius is proportional to the square root of compliance current. Similarly, FE in Figure 5(v) follows the same trend as that of Figure 5(iii), where the stable gap length increases with V_S or current. Note that compliance current is absent in our simulation, and the highest current in Figures 5(iii) and 5(v) is limited by the device dimensions and load resistance.

FE plots in Figures 5(iv) and 5(vi) shows that the thermal energy and volume term of the phase transformation energy dominates FE contributions. The thermal energy dominates for smaller radius/gap while the volume energy dominates for larger radius/gap thus yielding a minimum FE. Furthermore, the relative permittivity of the CF is assumed to be of

that of a metal however, it must be finite because CF contains insulating phase domains as well; this may add a contribution to the electrostatic energy.

5. Conclusions

Using a model of single phase cylinder CF, the fundamentals behind switching was numerically simulated via thermodynamic approach. A more elaborated CF structure (mixture of insulating phase and conducting phase) is needed to reproduce the device I-V characteristic that closely resembles a real device. The nanoscale thickness of the device also suggests the presence of tunneling current which might be a crucial factor in reproducing exact I-V. For next iteration, our aim is to combine RS with ONand OFF state I-V to reproduce the full RRAM I-V characteristics.

References

1. A. Fantini, et al., Intrinsic Switching Behavior in HfO_2 RRAM by Fast Electrical Measurements on Novel 2R Test Structures, *2012 4th IEEE International Memory Workshop, Milan*, pp. 1-4 (2012)
2. D. J. Wouters, et al., Analysis of Complementary RRAM Switching," *IEEE El. Dev. Letts.*, **33**, pp. 1186-1188 (2012)
3. Y. Y. Chen, et al., Understanding of the endurance failure in scaled HfO2-based 1T1R RRAM through vacancy mobility degradation," *2012 International Electron Devices Meeting, San Francisco, CA*, pp. 20.3.1-20.3.4 (2012)
4. S. Ambrogio, et al., Statistical Fluctuations in HfO_x Resistive-Switching Memory: Part I - Set/Reset Variability, *IEEE Trans. El. Dev.*, **61**, pp. 2912-2919 (2014)
5. S. Kim, et al., Physical electro-thermal model of resistive switching in bi-layered resistance-change memory, *Sci. Reps.*, **3**, pp. 1-6 (2013)
6. M. Bocquet, et al., Robust Compact Model for Bipolar Oxide-Based Resistive Switching Memories, *IEEE Trans. El. Dev.*, **61**, pp. 674-681 (2014)
7. B. Traor et. al., HfO_2-Based RRAM: Electrode Effects, Ti/HfO2 Interface, Charge Injection, and Oxygen (O) Defects Diffusion Through Experiment and Ab Initio Calculations, *IEEE Trans. El. Dev.*, **63**, pp. 360-368 (2016)
8. D. Ielmini, Resistive switching memories based on metal oxides: mechanisms, relaibility and scaling, *Semiconductor Sci. and Tech.*, **31**, pp. 063002 (2016)
9. V. Karpov, et al., Thermodynamic analysis of conductive filament, *Appl. Phys. Letts.*, **109**, pp. 093501 (2016)
10. V. G. Karpov, et al, Thermodynamics of phase transitions and bipolar filamentary switching in resistive random-access memory," in press, *Phys. Rev. Appl.*, **8**, pp.024028 (2017)
11. V. G. Karpov, et al., Field induced nucleation in phase change memory, Phys. Rev. B, **78**, pp. 052201 (2008)
12. A. Fantini, et al., Intrinsic switching variability in HfO_2 RRAM, *2013 5th IEEE International Memory Workshop, Monterey, CA*, pp. 30-33 (2013)
13. M.A. Panzer, et al., Thermal Properties of Ultrathin Hafnium Oxide Gate Dielectric Films, *IEEE El. Dev. Lett.*, **30**, pp. 1269-1271 (2009)
14. B. Govoreanu, et al., Complementary Role of Field and Temperature in Triggering ON/OFF Switching Mechanisms in Hf/HfO2 Resistive RAM Cells, *IEEE Trans. El. Dev.*, **60**, pp. 2471-2478 (2013)
15. E. Hildebrandt, et al., Controlled oxygen vacancy induced p-type conductivity in HfO_{2-x} thin films, *Appl. Phys. Letts.*, **99**, pp. 112902, (2011)
16. M.K. Samani, et al., Thermal conductivity of titanium aluminum silicon nitride coatings deposited by lateral rotating cathode arc," Thin Solids Films, **573**, pp. 108-112, (2013)
17. Carl L. Yaws. *The Yaws Handbook of Physical Properties for Hydrocarbons and Chemicals*, 2nd ed. Gulf Professional Publishing, Houston, TX (2015)
18. D. R. Lide, editor. *CRC Handbook of Chemistry and Physics*, 88thed., Taylor & Francis Group, Boca Raton, Florida (2008)
19. S. Privitera, et al., Microscopy study of the conductive filament in HfO2 resistive switching memory devices, *Microelectronic Engineering*, **109**, pp. 75-78 (2013)
20. E. Bozorg-Grayeli, et al., Thermal conductivity and boundary resistance measurements of GeSbTe and electrode materials using nanosecond thermoreflectance, *2010 12th IEEE Intersociety Conference on Thermal and Thermomechanical Phenomena in Electronic Systems, Las Vegas, NV,* pp.1-7 (2010)
21. C.Y. Chen, et al., "Novel Flexible and Cost Effective Retention Assessment Method for TMO Based RRAM," IEEE El. Dev. Lett., 37, pp. 1112-1115, (2016).

Acknowledgement

This work was supported in part by the Semiconductor Research Corporation (SRC) under Contract No. 2016-LM-2654. The authors are grateful to I. V. Karpov and R. Kotlyar for useful discussions.